Experimental and theoretical analysis of alginate-based hydrogel kinetics on sorption and desorption of atmospheric water vapor

M. Calò[1], **V. Gentile**[1]

[1]Energy Department, Politecnico di Torino, C.so Duca degli Abruzzi, 24, 10129, Italy

[*]Corresponding author: matteo.calo@polito.it

Abstract

Hydrogels are highly versatile polymer networks with the remarkable capability to uptake and release substantial amounts of water vapor, making them well-suited for utilization in atmospheric water harvesting applications. This investigation examines an alginate-based hydrogel from both experimental and theoretical perspectives, with a focus on identifying the key factors that contribute to the optimization of sorption/desorption cycles, including water capacity, kinetics, temperature, and vapor diffusion. The impact of the concentration of alginate networks and the reticulation initiator, calcium chloride, was assessed through an experimental investigation in which the material experienced controlled desorption and sorption cycles. The results revealed that higher concentrations of salt and lower levels of alginate within the composition led to enhanced sorption kinetics. The acquired data was subjected to fitting via three distinct models to quantify and compare the transport properties of various samples.

Keywords: Hydrogel, alginate, biopolymer, diffusion.

Introduction

Hydrogels are three-dimensional hydrophilic networks of polymer chains with the remarkable capability to uptake and release substantial amounts of water [1-2]. Due to their properties, hydrogels have been widely used in biomedical applications such as drug delivery [3-4] and tissue engineering [5]. Hydrogels can also be used for water remediation of oil contaminations [6], the removal of heavy metals [7-8], and other pollutants [9].
Currently, extensive research is being conducted on bio-derived hydrogels, to develop composite sorbents with superior hygroscopic properties for applications such as agriculture [10-11]. These hydrogels can reduce water consumption by conditioning the ground to augment water-holding capacity [12-13].
In particular, these hydrogels are being investigated for atmospheric water harvesting, where the biocompatibility of materials is crucial to produce drinkable water from the available moisture in the atmosphere [14-15]. Thermal cycling is utilized for this application, which requires heat input to regenerate the sorbent material. As with other thermally-driven sorption cycles, an optimal trade-off between the sorbent's water capacity and kinetics properties is critical. The regeneration temperature of the sorbent material is a crucial element that greatly impacts the overall energy efficiency of sorption/desorption cycles and diffusion rates. The duration of the sorption/desorption cycles is typically limited by diffusional resistance during both phases, whereas process-level maximization of kinetics is crucial to increase the number of cycles per day, resulting in higher moisture harvesting and water production. This analysis requires the use of the main theories of vapor diffusion through porous media, which involve mathematical modeling to predict and optimize moisture transport [16-17]. On the other hand, experimental techniques such as gravimetric analysis, dynamic vapor sorption, and scanning electron microscopy can also provide valuable information about the sorption and desorption behavior of the hydrogel, helping to improve the efficiency and effectiveness of moisture harvesting and water applications.

This work investigates the potentiality of a calcium alginate (CaAlg) hydrogel employing an experimental approach to evaluate the influence of $CaCl_2$ concentration and the amount of sodium alginate (NaAlg) on the hydrogel's equilibrium water uptakes and respective kinetic performance. CaAlg is a hydrogel obtained through the cross-linking of NaAlg with Ca^{2+} as a linking agent. NaAlg is the sodium salt of alginic acid, a natural polysaccharide extracted from brown seaweeds, and it is commonly used in food, pharmaceuticals, and other industrial applications where gelling agents are required. Ionotropic gelation is the mechanism by which crosslinking occurs between various chains of sodium alginate and Ca^{2+} cations in the hydrogel [18–20]. When the multiple chains of NaAlg come into contact with a solution containing divalent cations (e.g., $CaCl_2$ water solution contains Ca^{2+} ions) the Na^+ present in the chain is substituted with the cation. The presence of Ca^+ initiates the generation of free radicals that react with the crosslinking agent, forming a crosslinked polymer network usually called "egg-box" structure [21]. This analysis entails conducting experimental tests to determine the water vapor capture and release rates during the sorption and regeneration of the material and subsequently utilizing Fickian diffusion theory and the Linear Driving Force potential to derive and quantify the diffusion coefficients of the different hydrogel samples and formulations.

Materials and Methods

Sample Preparation and Testing

Following the aforementioned reaction, a setup was devised wherein a mixture of sodium alginate (NaAlg) and deionized water was dripped into a bath solution of calcium chloride ($CaCl_2$), resulting in the formation of beads comprising the final polymer. This composition was designed to isolate and assess the impact of only two parameters, NaAlg concentration and $CaCl_2$ concentration, based on the material preparation procedure.

Four different samples of NaAlg gel were prepared, mixing the mass of NaAlg with a fixed amount of deionized water (150 mL), obtaining two sets of samples respectively with 1%wt and 2%wt of NaAlg concentration. To obtain a homogeneous solution, the components were mixed with a magnetic stirrer at 500 rpm for two hours and then degassed under a vacuum between 200-500 mbar for 20 minutes. In parallel, 4 different $CaCl_2$/water solutions were prepared using 3 L of deionized water, two with 5%wt and the other two with 10%wt of anhydrous $CaCl_2$ (99% purity). The solution was mixed with a magnetic stirrer at 3000 rpm until the heat of the exothermic reaction was completely rejected to the environment, obtaining a final solution temperature equivalent to the lab environment. The NaAlg was ejected with a peristaltic pump through a 2 mm nozzle, dropping spheres of the gel directly into the reticulation bath. Once the gel interacts with the bath, the reticulation reaction occurs immediately for the outer surface of the sphere, preserving the geometry of the bead, while the complete reticulation of the internal part is constrained by the diffusion of Ca^{2+} ions through the radius of the beads. Then, to obtain a stabilized configuration, the solution was conventionally let rest for 24h. The resulting beads of CaAlg were drained and deeply rinsed with deionized water to remove the excess solution from the external surface. Finally, the beads were dried at 70 °C for 24 h removing the excess water resulting from their preparation. Four different samples were produced: sample S1 with NaAlg at 1%wt and $CaCl_2$ at 5%wt; sample S2 with NaAlg at 1%wt and $CaCl_2$ at 10%wt; sample S3 with NaAlg at 2%wt and $CaCl_2$ at 5%wt; sample S4 with NaAlg at 2%wt and $CaCl_2$ at 10%wt. Figure 1 reports a group of magnifications of the final result focused on the outer surface and the transversal section of sample S2, obtained through an FEI Quanta Scanning Electron Microscope. For each sample, the experimental tests followed the same procedure to evaluate both the maximum equilibrium water uptake at fixed conditions of regeneration/adsorption and the respective kinetics during both stages. Samples were first conditioned in a closed environment at 21°C and 50% of relative humidity, for more than 24 h to reach equilibrium with the conditioning

environment. Then samples were regenerated at 100 °C and ambient vapor pressure, in a thermal balance (KERN DBS60-3, with a linearity error of 3 mg) to evaluate mass variation during the transient, for 180 minutes. Right after the regeneration the sample was conditioned again in the closed environment and weighed every 10 minutes per 6 times, then every 15 minutes per 8 times, and finally every 30 minutes per 4 times, covering an entire period of 5 hours. This experimental procedure was repeated for each sample and results are reported in terms of water uptake in Figure (2).

Data Analysis Procedures

Experimental tests were analyzed using two different theoretical approaches: the Fickian diffusion (FD) theory and the Linear Driving Force (LDF) potential.
The FD model is based on the empirical observation of diffusive processes characterized by a proportionality between the mass flux J [kg/(m^{2}s)] and the opposite of the gradient of concentration C [kg/m^3] of a substance, fluid or gas, over a direction n, and the diffusivity D [m^2/s] of the diffusing substance in a specified medium [17]. Under the hypotheses of isotropic material, constant and not deformable volume, isothermal process, independency of diffusivity over time, and geometry with spherical symmetry (quantities do not vary with the angular coordinates, but only along the radius r [m]), the formulation of variation of concentration over time is:

$$\frac{\partial C}{\partial t} = \nabla \cdot (D \nabla C) = D \cdot \left(\frac{\partial^2 C}{\partial r^2} + \frac{2}{r} \cdot \frac{\partial C}{\partial r} \right) \tag{1}$$

Given the big difference between the diffusivity of the same substance in free air when compared to a porous sorbent (e.g., the diffusivity of water vapor in the air is around 2x10^{-5} m^2/s, while this value dramatically drops down to the order of 10^{-11} m^2/s when the medium is silica gel [22]) the boundary layer generated by the diffusion around the sorbent sphere can be neglected. Therefore, the most external surface of the sorbent brings immediately to the bulk concentration of the surrounding environment. As a consequence and in addition to the other mentioned hypotheses, the outer layer is considered in equilibrium with gas-side concentrations.
When the gas-side volume is sufficiently large, the presence of the adsorbent does not influence the gas concentration, which can be considered constant (C_∞), and the same concentration is found at the radius $r = R_p$ (radius of the particle of volume V_p). With the hypothesis of an initial uniform concentration different from zero, the initial and boundary conditions associated to eq. (1) are: $C|_{r,t=0} = C_0$; $C|_{r=R_p,t} = C_\infty$; $\left.\frac{\partial C}{\partial r}\right|_{r=0} = 0$. The solution is [17]:

$$C(r,t) = C_0 + (C_\infty - C_0) \cdot \left\{ 1 + \frac{2R_p}{\pi r} \cdot \sum_{n=1}^{\infty} \left[\frac{(-1)^n}{n} \cdot \sin\left(\frac{\pi n r}{R_p} \right) \cdot e^{-\pi^2 n^2 \left(\frac{D \cdot t}{R_p^2} \right)} \right] \right\} \tag{2}$$

Within eq. (2), the concentration depends on time and space. For practical applications the detailed knowledge of the spatial distribution is less useful than the total amount within the particle volume. For this reason, it is more convenient to formulate the eq. (2) in terms of the spatial average of sorbate concentration $\bar{C}$ as defined in equation (3) over a particle p, obtaining the resulting formulation in eq. (4):

$$\bar{C}(t) = \frac{1}{V_p} \cdot \int_p C(r,t) \cdot dV = \frac{3}{R_p^3} \cdot \int_0^{R_p} C(r,t) \cdot r^2 dr \tag{3}$$

$$\bar{C}(t) = C_0 + (C_\infty - C_0) \cdot \left\{ 1 - \frac{6}{\pi^2} \sum_{n=1}^{\infty} \left[\frac{e^{-\pi^2 n^2 \left(\frac{D \cdot t}{R_p^2} \right)}}{n^2} \right] \right\} \tag{4}$$

On the contrary respect to FD, the LDF model assumes the proportionality of the sorption driving force to the difference between the gas-side bulk concentration (C_∞) and the average sorbate concentration $\bar{C}(t)$ within the material:

$$\frac{d\bar{C}(t)}{dt} = K \cdot [C_\infty(t) - \bar{C}(t)] \tag{5}$$

K is a proportionality factor equal to:

$$K = \frac{F_0 \cdot D}{R_p^2} \tag{6}$$

, where F_0 is a shape factor, equal to 15 for spheres [23]. Note that the diffusivity D here reported is the very same diffusivity defined through Fick's first law. Applying the same initial and boundary conditions as for the FD, the LDF solution can be easily derived by integration of eq. (5), and it results:

$$\bar{C}(t) = C_0 + (C_\infty - C_0) \cdot \left(1 - e^{-\frac{F_0 \cdot D}{R_p^2} \cdot t} \right) \tag{7}$$

It is important to remember that eq. (7) follows by integrating eq. (5) under the hypothesis of constant coefficient K over time. In reality diffusivity depends, among the others, on temperature, which may change over time. It has been proposed a modified version (LDF_m) of the LDF model [22] in which the adimensional test temperature normalized to a reference value T_C and adimensional time $(D/R_p^2)t$ are corrected with exponents n and m, respectively, as in eq. (8):

$$\bar{C}(t) = C_0 + (C_\infty - C_0) \cdot \left(1 - e^{-F_0 \cdot \left(\frac{T}{T_C} \right)^n \left(\frac{D}{R_p^2} \cdot t \right)^m} \right) \tag{8}$$

Given the typical gravimetric approach used for experimental tests, the use of concentration as the main variable is less useful than the definition of water uptake (w) as the amount of sorbate within the material over the dry mass of the sorbent. When the volume of the particle is constant, the ratio of the instantaneous concentrations over the equilibrium concentration can be translated in terms of water uptake as:

$$\frac{\bar{C}(t) - C_0}{C_\infty - C_0} = \frac{w(t) - w_0}{w_\infty - w_0} = \begin{cases} \text{for Fickian Diffusion (FD):} & 1 - \frac{6}{\pi^2} \sum_{n=1}^{\infty} \left[\frac{e^{-\pi^2 n^2 \left(\frac{D \cdot t}{R_p^2} \right)}}{n^2} \right] \\ \text{for Linear Driving Force (LDF):} & 1 - e^{-\frac{F_0 \cdot D}{R_p^2} \cdot t} \\ \text{for modified LDF } (LDF_m): & 1 - e^{-F_0 \cdot \left(\frac{T}{T_c} \right)^n \cdot \left(\frac{D}{R_p^2} \cdot t \right)^m} \end{cases}$$

Since the experimental campaign involved adsorptions and regenerations at constant temperatures (21 °C and 100 °C respectively), for the purpose of this paper it is supposed $(T/T_C)\hat{}n = 1$. Thus, the modified version of LDF (LDF_m) only involves parameters D and m. Additionally, the formula can be extended to desorption, making it even more useful.
These three models (FD, LDF, and LDF_m) have been applied to the experimental results reported in the following section, using a fitting procedure. The main purpose is to evaluate and compare the diffusive coefficient to discuss the influence of the two main parameters analyzed in the design of the experiment process: the concentration of the crosslinking initiator $CaCl_2$, and the concentration of alginate monomers chains NaAlg. Further on, models are used to analyze the influence of cycle duration on the maximization of the water uptake variation over time.

The quantification of the model parameters was performed through the minimization of the least square root error [24]. This consists in searching for the values of the model parameters which minimize the sum of the squares of the differences between each experimental point and the model output evaluated at the same input. Given a generic function f to model experimental data, dependent on time and on multiple parameters such as $f(t, p_1, p_2, \dots, p_M)$, the error function err is:

$$err(p_1, p_2, \dots, p_M) = \sum_{i=1}^{N} [f(t_i, p_1, p_2, \dots, p_M) - y_i]^2$$

, where (t_1, y_1), (t_2, y_2), $\dots$, (t_N, y_N) are the coordinates of the N experimental points of the test to be fitted, while err is a function of the sole model parameters. In this research the function f is the water uptake w while t is the time of the experiment. The list of parameters, as well as the function w, change according to the selected model:

- for LDF, $M = 1$, $p_1 \equiv D$
- for LDF_m, $M = 2$, $p_1 \equiv D$, $p_2 \equiv m$
- for FD, $M = 1$, $p_1 \equiv D$.

The identification of the best fitting model parameters follows the objective research of values $p_1, p_2, \dots, p_M$ which minimize err. The minimization algorithm used is the Nelder-Mead simplex [25-26], in particular:

- for the fitting of the LDF model, it was searched the positive value of D which minimizes the function $err(D)$, starting from a 1st-iteration value of $D = 10^{-11}\ m^2/s$;
- for the fitting of the LDF_m model, the positive values of D and m which minimize the function $err(D, m)$, starting from 1st-iteration values of $D = 10^{-11}\ m^2/s$ and $m = 1.0$;
- for the fitting of the FD model, the positive value of D which minimizes the function $err(D)$, starting from a 1st-iteration value of $D = 10^{-11}\ m^2/s$.

Discussion and Results

In Figure 1 three SEM magnifications show the external surface of a bead of CaAlg dried polymer and its transversal section. The polymer has a pseudo spherical shape, with an equivalent radius of $0.969\ mm$, and has a highly rugged surface with multiple openings. Additionally, concentric traces are visible from the outer surface to the inner surface, presumably linked to the progression of the diffusion front and crosslinking of Ca^{2+} ions. The openings start from the outer surface, and they go through the radial direction involving a thickness lower than 200 µm. In the grain inner section, a predominantly solid microstructure exists, apart from the occurrence of

regions exhibiting significant void spaces which can be attributed to inadequate removal of air during the degassing process.

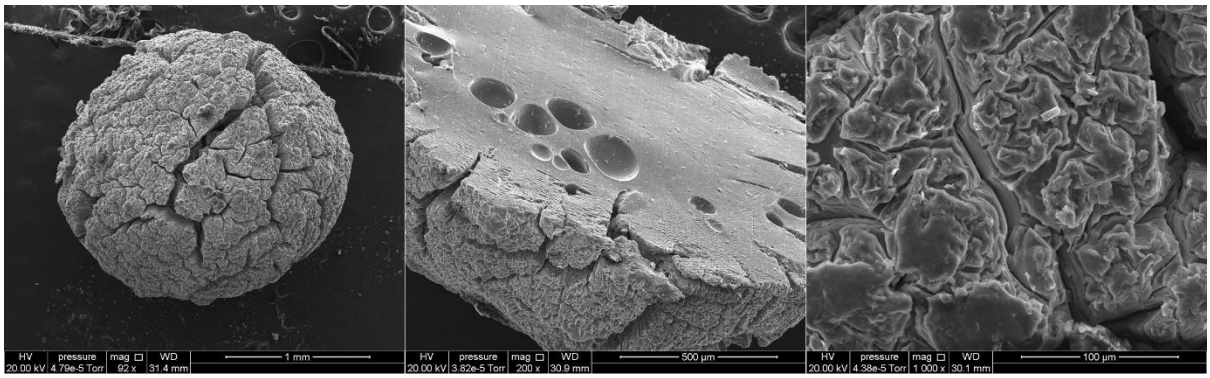

Figure (1). SEM magnifications of a grain of sample S2. (left) a view of the external surface of a pseudo-spherical particle of dried CaAlg; (center) transversal section of a particle of dried CaAlg with the same composition of S2; (right) magnification of the image at the center, focused on the external surface structure.

Figure (2) displays the results of adsorption and regeneration tests as variations in water uptake. The graph on the left presents the results of the test conducted on sample S1, which consisted of a desorption cycle (first 3 hours) followed by an adsorption cycle (next 5 hours), illustrated by a solid line. The points on the adsorption curve correspond to the experimental measurements, while during desorption, the mass of the sample was measured every 5 seconds. The adsorption process was terminated after 5 hours before the material attained its equilibrium mass, which requires approximately 12 hours. However, after 5 hours, the water uptake reached a value w_{5h} of approximately 80% of the equilibrium value, as shown in Table 1.
The dotted line depicts the relative humidity (RH) during the experiment, while the RH after the box is left to evolve for a sufficiently long time (RH_{eq}) is illustrated above with the horizontal line. The RH in the conditioning chamber varies over time because the box was opened to place the sample and the conditioning chamber is not large enough to avoid being affected by the adsorption process. The combination of these factors causes the equilibrium concentration experienced by the material to change over time. This suggests that the use of the models should involve a time-dependent function of $C_\infty(t)$ rather than a constant value. The graph on the right of the same figure reports the same kind of test for all four different samples.

The sample composition affects the adsorption and regeneration behaviors. For example, sample S2 shows a greater equilibrium water uptake, while sample S3 has a weaker adsorption capacity. Sample S1 performs better in desorption, exhibiting a steeper behavior. Increasing the $CaCl_2$ content (at a fixed alginate content) the equilibrium value increases. The same conclusion applies to the comparison of S2 with S1 and S4 with S3. Conversely, increasing the alginate content (at a fixed salt content) reduces the steepness of the adsorption process and the equilibrium water uptake at regime conditions, as shown by the comparison between tests S2 and S4, and tests S1 and S3.
It should be noted that the steepness of a sorption/desorption curve is correlated to the diffusive coefficient value as well as to the equilibrium value. If the LDF is used to model the phenomenon, the D/R_p^2 parameter acts as the inverse of a characteristic time τ in a generic exponential expression in the form: $x(t) = A + B \cdot \exp(-t/\tau)$. Sorption/desorption tests with steeper behavior at fixed equilibrium value will be fitted using lower transient characteristic times, which in turn correspond to higher diffusive coefficients.

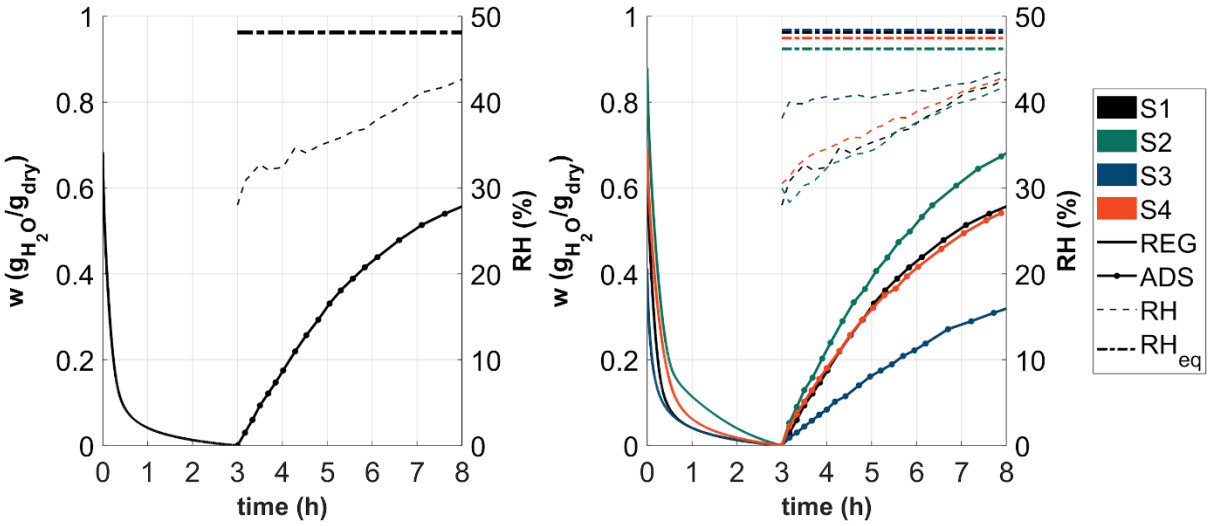

Figure (2). (left) test results of sample S1: time t on the x-axis, water uptake w on the left y-axis, relative humidity RH on the right y-axis; (right) comparison of test results for all the samples S1, S2, S3, S4. The graphs report a regeneration at 100°C and adsorption at 21°C and RH=50%.

Table 1 shows the numerical values of water uptakes alongside the initial and equilibrium RH values measured in the conditioning chamber during the adsorption process. The value of w at the beginning of the regeneration is denoted as w_0, which is equivalent to the equilibrium value that the sample in adsorption would have reached if the experiment had not been interrupted after 5 hours. For each sample, the water uptake at the end of the regeneration process corresponds to the initial water uptake of the adsorption process, given the experimental procedure. This value was assumed as the "zero" point to define the dry mass and for the definition of water uptakes.

Table 1. Initial and final water uptakes and RHs, for tests S1, S2, S3 and S4.

Test	REGENERATION	ADSORPTION		
	$w_0\ (g/g)$	$w_{5h}(g/g)$	$RH_0(\%)$	$RH_{eq}(\%)$
S1	0.683	0.562	28.0	48.1
S2	0.880	0.706	30.0	46.2
S3	0.412	0.326	38.1	48.4
S4	0.695	0.542	30.5	47.5

The analytical solutions provided above (FD, LDF, LDF_m) are valid for a fixed geometry where the radius is constant, while a real process on hydrogel spheres, or other polymers, may lead to a significant change in the volume of particles. For this reason, and to reach better fittings between the models and real data, the R_p was the average (avg) value of the equivalent spherical particle over the entire transient:

$$V_{avg} \approx \frac{V_0 + V_\infty}{2} \quad \rightarrow \quad R_p \equiv R_{p,avg} = \sqrt[3]{\frac{R_0^3 + R_\infty^3}{2}}$$

Where the subscripts 0 and ∞ represent the initial and the equilibrium condition of each adsorption and regeneration stage. One average value between the four samples was used to fit regenerations and one for adsorptions. In particular, the average value of the radius during regeneration was

$R_{p,avg,reg} = 0.937\ mm$ ($\sigma_{R,reg} = 0.130\ mm$), while the average value of the radius during adsorption was $R_{p,avg,ads} = 1.12\ mm$ ($\sigma_{R,ads} = 0.097\ mm$).

The proposed analytical solutions assume constant concentration on the gas-side. However, because changes in relative humidity affected the concentration in the conditioning chambers, this assumption is not acceptable for this kind of experiment. For this reason, the FD model was properly manipulated by incorporating a step-wise change in gas-side concentration that reflects the varying relative humidity (RH) levels during the experiment. Initially, the concentration would be lower than the equilibrium value due to lower RH levels, but it would increase as the RH levels rise. Assuming that the relationship between concentration C_∞ and RH is linear, one could model the increase in $C_\infty(t)$ over time as being proportional to RH(t). Thus, when RH=RH_{eq}, C_∞ would be equal to w_∞.

The time interval is subdivided into N steps, and the FD model is used in its original expression at each step with the same diffusivity to evaluate the new increment in concentration. By increasing the resolution of the step-wise approach (by increasing the number N of discrete subdivisions of testing time) the resulting approximation is expected to improve. This is confirmed by Figure (3), which shows on the left how the step-wise FD (swFD) model better fits experimental data as N increases. For N=1, the swFD model degenerates into an ordinary FD model applied on the whole test time interval, with a consistent overestimation of the water uptake during the first part of the transient, and a symmetrical underestimation for the second part of the transient. When the number N of discrete increases in RH is set to 2 the approximation improves, as the model predicts a lower equilibrium value at the start of the adsorption process. As N increases, the curve becomes even closer to the experimental data, and the fitted value of diffusivity D (as shown in Figure (3) on the right for all four tests) varies more slowly, except for numerical oscillations at higher N resulting from interpolation algorithm. The value of D for N=100 is assumed as the outcome of the fitting procedure with the swFD model. The deviation of the curve from the experimental data may be due to the violation of other hypotheses of the FD model, such as constant particle volume and constant diffusivity, as well as the assumption about the linear relationship between C_∞ and RH.

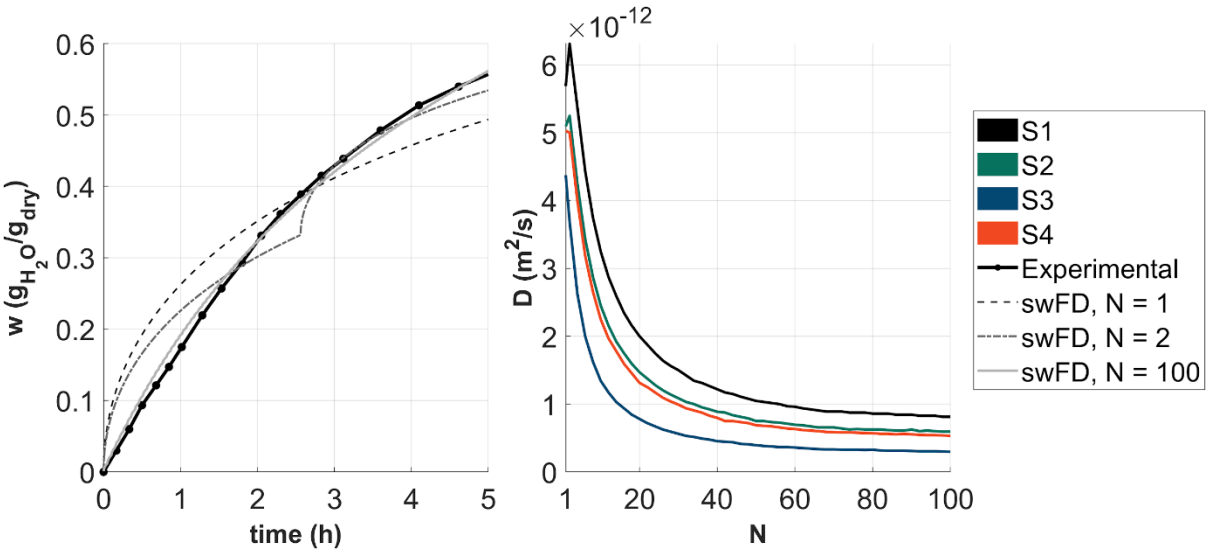

Figure (3). (left) experimental data of test S1 and step-wise FD (swFD) model for a different number of steps N; (right) change in the fitted value of coefficient D with increasing N, for tests S1, S2, S3, S4. For N=1, swFD is equivalent to the original FD model.

The final results of the FD model calculations are reported in Table 2 and Table 3, where the infinite sum was approximated using its first 300 items since the contributions beyond the first 50 terms of the sum were insignificant. Indeed, the additional iterations after the 50th affect the total

water uptake with a magnitude of approximately 0.01 g/g, and similarly, the contributions on the fitted diffusion coefficient are negligible dropping below 1e-14 m^2/s.

The modified equation of LDF is versatile and can be applied to fit experimental data for both adsorption and regeneration. However, it should be noted that the coefficients in the LDF_m model do not have an immediate physical interpretation. Indeed, the corrective coefficient causes the deformation of the resulting curve to better fit the experimental data. The introduction of new mathematical degrees of freedom reduces the overall error, but at the expense of an unclear interpretation of the diffusivity coefficient D. This creates consistency problems when it is carried out a comparison of diffusivities between the different modelling approaches. For this reason, it is more appropriate to use a model based on physical principles, such as the FD or classic LDF, which have a clear physical interpretation.

Figure (4), for example, reports the fitting obtained through each of the different models (LDF, LDF_m, and swFD) shown above, in comparison with the experimental data. The absolute error over time is shown below.

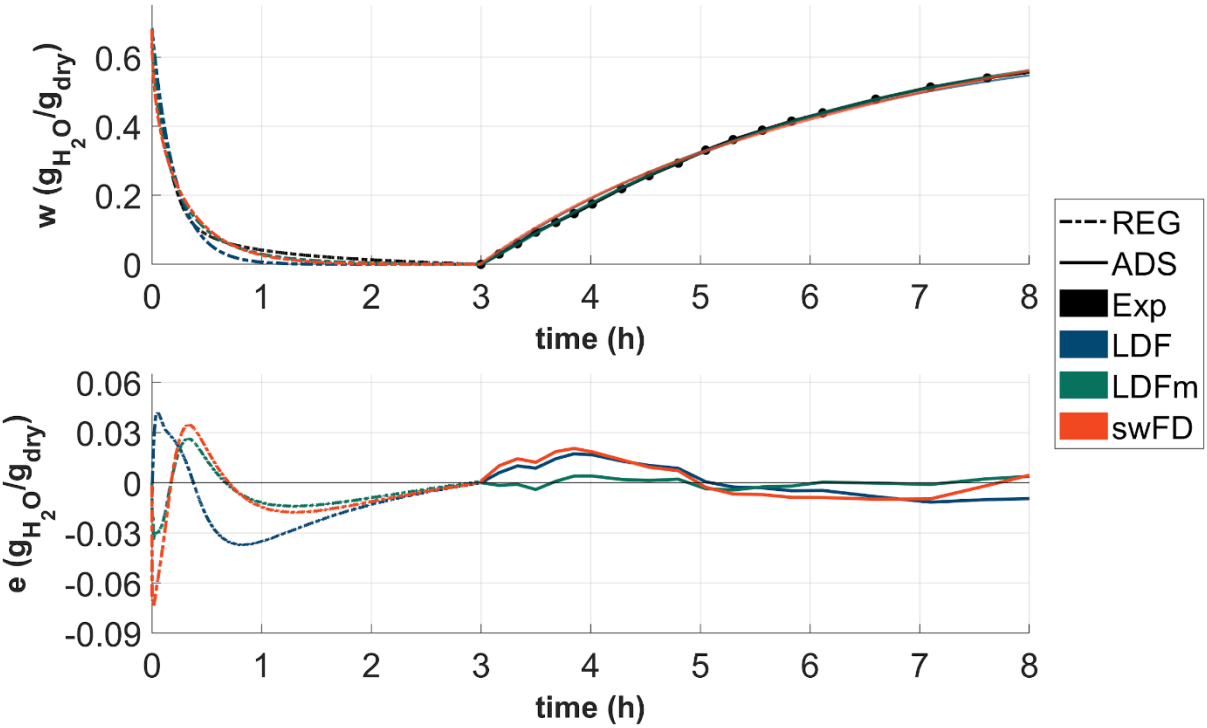

Figure (4). (above) LDF, LDF_m, and $swFD_{N=100}$ models in comparison and against the experimental data of the test on sample S1; (below) absolute error over time made by each model, in regeneration and adsorption.

It can be observed that all three models perform well in modeling the adsorption process, while the regeneration phase exhibits higher errors. The LDF_m model is the most precise in both adsorption and desorption, but this could be simply related to the introduction of an additional degree of freedom (i.e., the exponent m) with respect to the other model versions.

Table 2 reports the numerical values of diffusion coefficient D obtained from fitting the different models with regeneration tests (REG), while Table 3 reports the same data for adsorption tests (ADS). Additionally the average absolute error $\bar{e}$ (average of the instantaneous differences between the estimated and the experimental values) and its standard deviation over time σ_e are reported.

Higher values of D are associated with samples containing less alginate (S1 and S2), coherently with what was observed above. Such samples show a steeper behavior, i.e., a faster sorption/desorption process. Regarding the fitting of the LDF_m model, the corrective coefficient

m was observed to have specific values for regeneration and adsorption. For the regeneration, the tests S1, S2, S3, and S4 had m values equal to 0.708, 0.687, 0.555, and 0.795 respectively. On the other hand, for adsorption m had values of 1.09, 1.00, 1.16, and 0.996 respectively. It is noteworthy that in these last cases the coefficients reached proximity to unity values. This indicates a scenario where the ordinary LDF model is already more than sufficient to effectively represent the material's behavior. For example, this is evident in the test of S2 where the value of m rounded to the 2nd decimal place is 1.00, as consequence the value of D coincides with the one evaluated with the simple LDF. On the contrary, desorption requires a more substantial adjustment of the coefficient m to minimize the error that occurs during the LDF fitting process. The reason why adsorption is better suited to LDF modeling than desorption may be attributed to the fact that the linear potential is more suitable for simulating the sorption phenomena at lower temperatures.

Table 2. REG diffusion coefficients and errors resulting from LDF, $LDF_{m,}$ and $swFD_{N=1}$ fittings.

Test	LDF			LDF_m			swFD		
	D $\left(\frac{m^2}{s}\right)$	$\bar{e}$ $\left(\frac{g}{g}\right)$	σ_e $\left(\frac{g}{g}\right)$	D $\left(\frac{m^2}{s}\right)$	$\bar{e}$ $\left(\frac{g}{g}\right)$	σ_e $\left(\frac{g}{g}\right)$	D $\left(\frac{m^2}{s}\right)$	$\bar{e}$ $\left(\frac{g}{g}\right)$	σ_e $\left(\frac{g}{g}\right)$
S1	7.6 e-11	-1.29 e-2	1.83 e-2	2.7 e-11	-5.05 e-3	1.10 e-2	6.8 e-11	-6.65 e-3	1.62 e-2
S2	4.4 e-11	-1.95 e-2	3.72 e-3	1.4 e-11	-3.33 e-3	1.82 e-2	3.9 e-11	-5.94 e-3	2.56 e-2
S3	6.5 e-11	-1.14 e-2	2.21 e-2	8.9 e-12	-2.87 e-4	4.74 e-3	5.5 e-11	-4.64 e-3	1.14 e-2
S4	4.8 e-11	-9.23 e-3	1.65 e-2	2.5 e-11	-3.19 e-3	8.29 e-3	4.4 e-11	-2.57 e-3	1.95 e-2

Table 3. ADS diffusion coefficients and errors resulting from LDF, $LDF_{m,}$ and $swFD_{N=100}$ fittings.

Test	LDF			LDF_m			swFD		
	D $\left(\frac{m^2}{s}\right)$	$\bar{e}$ $\left(\frac{g}{g}\right)$	σ_e $\left(\frac{g}{g}\right)$	D $\left(\frac{m^2}{s}\right)$	$\bar{e}$ $\left(\frac{g}{g}\right)$	σ_e $\left(\frac{g}{g}\right)$	D $\left(\frac{m^2}{s}\right)$	$\bar{e}$ $\left(\frac{g}{g}\right)$	σ_e $\left(\frac{g}{g}\right)$
S1	7.5 e-12	2.66 e-3	9.61 e-3	9.5 e-12	2.35 e-5	2.67 e-3	8.1 e-13	4.10 e-3	1.13 e-2
S2	7.0 e-12	3.34 e-3	5.51 e-3	7.0 e-12	-8.21 e-4	4.56 e-3	5.9 e-13	5.66 e-4	5.92 e-3
S3	6.3 e-12	3.63 e-3	9.35 e-3	9.3 e-12	-8.14 e-4	3.62 e-3	3.0 e-13	3.38 e-3	8.89 e-3
S4	7.0 e-12	-2.11 e-3	3.77 e-3	7.0 e-12	-7.25 e-4	4.01 e-3	6.3 e-13	-9.37 e-4	3.86 e-3

Even if its parameters do have not a direct physical interpretation, the LDF_m best models the curves of water uptake over time. For this reason, it has been selected to simulate the behavior of the material when it is subject to cyclic desorption and adsorption processes.
For example in real applications requiring the harvesting of atmospheric water vapor, the thermal cycle can undergo short fixed times, and repeated many times per day. As a result, materials will hardly reach equilibrium conditions over multiple cycles. Nonetheless, after a few repetitions, the process will reach a regime behavior in which the water uptake, at the beginning of each regeneration, is reduced to a new value lower than the maximum potential related to actual atmospheric conditions. Here, the chosen durations of regeneration and adsorption cycles are such that the decrease in water uptake during regeneration is identical to its increase during adsorption. Initial water uptake, regeneration time, and adsorption time at a given regime are not independent, as one follows the other two (once they are fixed). If the initial water uptake is established as a percentage of the equilibrium water uptake (e.g. 85% of the equilibrium value), the variation in water uptake (Δw) observed during each cycle reaches a regime which is solely determined by the regeneration time and cycling conditions (such as temperatures and relative humidities), as evidenced by the results in Figure 5 (graph on the left).
Moreover, the total cycling time Δt, which encompasses both regeneration and adsorption processes, is limited by the regeneration time since adsorption only restores the material's water uptake to the value obtained at the beginning of regeneration. It can be useful to evaluate the quantity of water uptake rate (i.e., the ratio between the Δw and Δt of each cycling option, for each partial regeneration time), which is a crucial performance metric if the goal of the application is to maximize the water vapor collection in a fixed duration. In Figure (5) (on the right) this metric is plotted against each possible partial regeneration time, for different initial water uptakes.

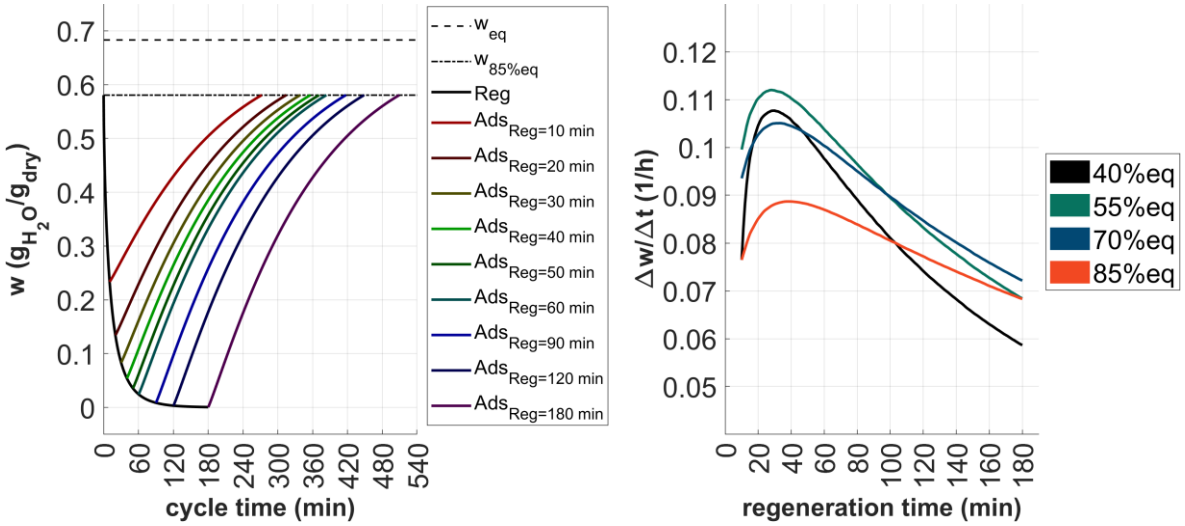

Figure (5). (left) settled cycling curves (simulated through LDF_m for regeneration at 100°C and adsorption at 21°C and RH=50%) at different fixed regeneration times, in fixed environmental conditions and for sample S1; (right) the water uptake rate on the y-axis plotted against each partial chosen regeneration time, for different initial water uptakes expressed as a fraction of the equilibrium value.

The graph on the right of Figure (5) reveals two interesting observations. Firstly, the curve of water uptake rate varies with the initial value (expressed as a percentage of the equilibrium value), with a maximum reached around 55% of w_{eq}. Secondly, each curve achieves a peak value for an intermediate partial regeneration time of around 30-35 minutes. These effects are attributed to the changing steepness of the regeneration and adsorption curves. An optimal regeneration time and an optimal reg starting value can be identified such that the regeneration is long enough to yield a high Δw but not too long to result in a high Δt due to the adsorption time.

Conclusions

This paper explored the influence of composition on the sorption and desorption performances of a family of alginate-based hydrogels and how the kinetics of such processes can be modeled.

It was observed that higher contents of calcium chloride in the composition of the hydrogel imply better adsorption capacities; higher contents of alginate in the composition imply, on the other hand, worse adsorption capacities and longer characteristic times: this is confirmed by the values of the fitted diffusivities, which are higher in case of samples containing less alginate (S1 and S2).

The models used to fit diffusivity were the Fickian diffusion (FD), the Linear Driving Force (LDF), and a modified version of the Linear Driving Force (LDF_m). The latter resulted in the most accurate description of the kinetics of both regeneration and adsorption, but the resulting diffusivity value may be distorted by the introduction of a corrective coefficient, which does not allow a simple physical interpretation of the results. On the other hand, the FD and the LDF models both provided diffusivity values of the order of magnitude 10^{-11} m^2/s in regeneration and values around 10^{-13} - 10^{-12} m^2/s in adsorption.

The LDF_m model, given its mathematical accuracy, was used to simulate the cyclic behavior of one of the studied hydrogels, when non equilibrium cycles are applied with a fixed initial water uptake and at various regeneration times. The water uptake rate was defined as the amount of Δw gained in one complete cycle divided by the cycle time: such quantity is a key indicator in an application that requires to maximize the amount of water extracted in a fixed amount of time. The simulations allowed us to find that it exists an optimal initial water uptake, as well as an optimal regeneration time for each initial water uptake, in order to maximize the water uptake rate.

Future research can investigate the potential of enhancing the adsorption and desorption performance of alginate-based hydrogels by incorporating other materials and additives, while also focusing on developing more accurate models that can account for transient environmental factors, volumetric variations, and the presence of multiple materials.

Acknowledgments

We would like to express our gratitude to Princeton University, and in particular to Dr. M. Bozlar for providing the Scanning Electron Microscopy (SEM) images used in this research. The use of these images was instrumental in our study and greatly enhanced the quality of our results.

References:

[1] E. Caló and V. V. Khutoryanskiy, “Biomedical applications of hydrogels: A review of patents and commercial products,” Eur. Polym. J., vol. 65, pp. 252–267, 2015.

[2] N. A. Peppas, P. Bures, W. Leobandung, and H. Ichikawa, “Hydrogels in pharmaceutical formulations,” Eur. J. Pharm. Biopharm., vol. 50, no. 1, pp. 27–46, 2000.

[3] K. Y. Lee and D. J. Mooney, “Alginate: Properties and biomedical applications,” Prog. Polym. Sci., vol. 37, no. 1, pp. 106–126, 2012.

[4] M. N. V. R. Kumar, “A review of chitin and chitosan applications,” React. Funct. Polym., vol. 46, pp. 1–27, 2000.

[5] J. L. Drury and D. J. Mooney, “Hydrogels for tissue engineering: Scaffold design variables and applications,” Biomaterials, vol. 24, no. 24, pp. 4337–4351, 2003.

[6] Z. Xue et al., “A novel superhydrophilic and underwater superoleophobic hydrogel-coated mesh for oil/water separation,” Adv. Mater., vol. 23, no. 37, pp. 4270–4273, 2011.

[7] O. Ozay, S. Ekici, Y. Baran, N. Aktas, and N. Sahiner, "Removal of toxic metal ions with magnetic hydrogels," Water Res., vol. 43, no. 17, pp. 4403–4411, 2009.
[8] F. Ge, M. M. Li, H. Ye, and B. X. Zhao, "Effective removal of heavy metal ions Cd 2+, Zn 2+, Pb 2+, Cu 2+ from aqueous solution by polymer-modified magnetic nanoparticles," J. Hazard. Mater., vol. 211–212, pp. 366–372, 2012.
[9] X. Zhou, F. Zhao, Y. Guo, B. Rosenberger, and G. Yu, "Architecting highly hydratable polymer networks to tune the water state for solar water purification," Sci. Adv., vol. 5, no. 6, pp. 1–8, 2019.
[10] M. R. Guilherme et al., "Superabsorbent hydrogels based on polysaccharides for application in agriculture as soil conditioner and nutrient carrier : A review," Eur. Polym. J., vol. 72, pp. 365–385, 2015.
[11] B. Ni, M. Liu, S. Lü, L. Xie, and Y. Wang, "Environmentally friendly slow-release nitrogen fertilizer," J. Agric. Food Chem., vol. 59, no. 18, pp. 10169–10175, 2011.
[12] B. Song, H. Liang, R. Sun, P. Peng, Y. Jiang, and D. She, "Hydrogel synthesis based on lignin/sodium alginate and application in agriculture," Int. J. Biol. Macromol., vol. 144, pp. 219–230, 2020.
[13] N. Thombare, S. Mishra, M. Z. Siddiqui, U. Jha, D. Singh, and G. R. Mahajan, "Design and development of guar gum based novel, superabsorbent and moisture retaining hydrogels for agricultural applications," Carbohydr. Polym., vol. 185, no. October 2017, pp. 169–178, 2018.
[14] F. Zhao, X. Zhou, Y. Liu, Y. Shi, Y. Dai, and G. Yu, "Super Moisture-Absorbent Gels for All-Weather Atmospheric Water Harvesting," Adv. Mater., vol. 31, no. 10, pp. 1–7, 2019.
[15] R. Li, Y. Shi, M. Alsaedi, M. Wu, L. Shi, and P. Wang, "Hybrid Hydrogel with High Water Vapor Harvesting Capacity for Deployable Solar-Driven Atmospheric Water Generator," Environ. Sci. Technol., vol. 52, no. 19, pp. 11367–11377, 2018.
[16] D. M. Ruthven, "Douglas M. Ruthven. Principles of Adsorption and Adsorption processes.", 1984.
[17] J. Crank, "The mathematics of diffusion", Clarendon Press Oxford, 2nd ed., 1975.
[18] C. Hu, W. Lu, A. Mata, K. Nishinari, and Y. Fang, "Ions-induced gelation of alginate: Mechanisms and applications," Int. J. Biol. Macromol., vol. 177, pp. 578–588, 2021.
[19] S. Paoletti and I. Donati, "Comparative Insights into the Fundamental Steps Underlying Gelation of Plant and Algal Ionic Polysaccharides: Pectate and Alginate," Gels, vol. 8, no. 12, 2022.
[20] P. A. Kallenberger and M. Fröba, "Water harvesting from air with a hygroscopic salt in a hydrogel–derived matrix," Commun. Chem., vol. 1, no. 1, pp. 6–11, 2018.
[21] I. Braccini and S. Pérez, "Molecular basis of Ca2+-induced gelation in alginates and pectins: The egg-box model revisited," Biomacromolecules, vol. 2, no. 4, pp. 1089–1096, 2001.
[22] I. I. El-Sharkawy, "On the linear driving force approximation for adsorption cooling applications," Int. J. Refrig., vol. 34, no. 3, pp. 667–673, May 2011.
[23] E. Glueckauf, "Theory of chromatography. PART lO.-FORMULA FOR DIFFUSION INTO SPHERES AND THEIR APPLICATION TO CHROMATOGRAPHY," Trans. Faraday Soc. Superseded by J. Chem. Soc., Faraday Trans., I II, vol. 51, no. 3851, p. 220, 1955.
[24] Bickel J.P., Doksum A.K., "Mathematical statistics", vol. 1. 2013.
[25] J. C. Lagarias et al., "Convergence properties of the Nelder-Mead simplex method in low dimensions", Society for Industrial and Applied Mathematics, 1998.
[26] J. A. Nelder and R. Mead, "A simplex method for function minimization", The Computer Journal, vol. 8, 1965.